Hindawi Publishing Corporation
Journal of Nanomaterials
Volume 2013, Article ID 157474, 6 pages
http://dx.doi.org/10.1155/2013/157474

Research Article

Preparation and Oxygen Permeability of $BaCo_{0.7}Fe_{0.2}Nb_{0.1}O_{3-\delta}$ Membrane Modified by $Ce_{0.8}Y_{0.2}O_{2-\delta}$ Porous Layer on the Air Side

Yuan Qiang,[1] Zhen Qiang,[1,2] and Li Rong[2]

[1] *School of Materials Science and Engineering, Shanghai University, Shanghai 200072, China*
[2] *Nano Science and Technology Research Center, Shanghai University, Shanghai 200444, China*

Correspondence should be addressed to Zhen Qiang; qzhen@staff.shu.edu.cn

Received 31 August 2013; Accepted 10 October 2013

Academic Editor: Amirkianoosh Kiani

$BaCo_{0.7}Fe_{0.2}Nb_{0.1}O_{3-\delta}$ (BCFN) dense ceramic membrane with submicron-$Ce_{0.8}Y_{0.2}O_{2-\delta}$ (YDC) porous layer was investigated by the partial oxidation of coke oven gas (COG) in hydrogen production. XRD analysis showed this composite had good stability and no chemical reaction at high temperature. SEM and TEM characterization further showed BCFN membrane was uniformly modified by YDC porous layer (about 5~6 μm thickness) formed by the accumulation of relative nanoparticles. At the respective COG flux and air flux of 108 mL/min and 173 mL/min, the oxygen permeation flux of BCFN modified by submicron-YDC porous layer reached 16.62 $mL \cdot min^{-1} \cdot cm^{-2}$, which was about 23.5% higher than that of pure BCFN membrane. Therefore, submicron-YDC porous layer obviously improved the oxygen permeation flux of BCFN membrane and its stability at 875°C.

1. Introduction

Partial oxidation of methane (POM) reforming technology is considered as one of the most economic and logical methods to produce syngas. Through further transforming and separating the formed syngas, then hydrogen can be further obtained. Coke oven gas (COG), a by-product which was generated in the process of producing coke from coal at the high temperature of 800°C, contains 30–40% CH_4 and is one of the most promising sources for hydrogen production [1]. Meanwhile, dense ceramic oxygen permeable membranes are widely used to separate oxygen from air at elevated temperatures with infinite permeation selectivity. These membranes are usually made from mixed oxygen ionic and electronic conductor (MIEC) and derived from perovskite-type (ABO_3) materials since ABO_3 materials display oxygen semipermeability due to their MIEC. Considering the two distinct processes which influence the rate of oxygen transport (bulk vacancy diffusion and surface exchange kinetics [2]), $BaCo_{0.7}Fe_{0.2}Nb_{0.1}O_{3-\delta}$ (BCFN) membranes [3–5] show excellent oxygen permeability among the large variety of structural ABO_3 materials [6–14]. The rate of oxygen transport through the membrane is regulated by two distinct processes, bulk vacancy diffusion and surface exchange kinetics [2]. Furthermore, it also pushes the oxygen permeation rate limiting step near the side of the surface kinetics by reducing the thickness of membranes.

In order to improve the surface kinetics of oxygen transport, surface modification of the membrane with a higher surface exchange rate layer is a feasible way. This method increases the rate of surface kinetic reactions, which is beneficial for higher oxygen permeation rates under surface exchange or mixed controlled situations [4]. Recently, some researchers have played their great effort on surface modification of the membrane [15–17]. Although it is very important to modify the membrane on the reductive side, the surface modification on the air side is rarely reported. Ceria electrolytes exhibit superior ionic conductivity at lower temperature ranges (773–973 K) [18–21]. The high specific surface area and high ionic conductivity of submicron-$Ce_{0.8}Y_{0.2}O_{2-\delta}$ may obviously improve the surface kinetic reactions and oxygen permeability.

In this paper, BCFN membranes were modified by submicron-$Ce_{0.8}Y_{0.2}O_{2-\delta}$ (YDC) porous layer on the air side. XRD, SEM, and TEM were used to characterize the BCFN membranes with and without YDC modification. The influences of YDC modification on the surface kinetics and oxygen permeation rates of BCFN membranes were also systematically analyzed.

2. Experimental

2.1. Preparation of BCFN Powders, YDC Nanopowders, and BCFN-YDC Ceramics. BCFN powders were prepared by solid-state reaction method as described in [19]. BCFN membranes (Φ = 20 mm, d = 1.5 mm) were prepared by uniaxial pressing BCFN powders at 200–250 MPa and then dried at 110°C for 24 h. The green bodies were further sintered at 1110°C for 8 h in air (a heating rate of 5°C/min) to obtain dense membrane. The membranes were polished to 1 mm thick before they were used.

YDC nanopowders were synthesized by the reverse titration chemical coprecipitation method as described in [22–24]. Nano-YDC porous layer was coated on one side of BCFN membranes by using the dipping method [2, 25–27]. It was then treated at 1000°C for 2 h. The BCFN membrane with thin submicron-YDC porous layer was marked as BCFN-YDC.

2.2. Characterization. Phases of BCFN powders, YDC nanopowders, and BCFN-YDC membrane were characterized by X-ray diffraction (D/max-2550 X-ray diffractometer, Rigaku, Japan) using CuK_α radiation (λ = 0.154178 nm). A continuous scan mode was applied to collect data in $10^\circ \le 2\theta \le 90^\circ$ with a 0.02° step size and a 4°/min scanning rate. The crystalline size of YDC nanopowders was calculated by the Scherrer equation $D = 0.89\lambda/(B \cdot \cos\theta)$, where B is the full width at half maximum of Bragg peaks.

Micrograph of YDC nanopowders was observed using transmission electron microscopy (TEM, 200CX transmission electronic microscope, Japan). Micrograph of BCFN membrane and BCFN-YDC membrane was observed by scanning electron microscopy (SEM, JSM-6700F high resolution scanning electronic microscope, Japan). The adhesion of BCFN membrane and YDC porous coating was tested by ultrasound machine (B3500S-DTH, 140 W, 42 kHz).

2.3. Oxygen Permeation Measurements. The diagram of membrane reactor is given in Figure 1. BCFN membrane with 17 mm diameter and 1.0 mm thickness was placed in the quartz tube. A silver ring was used as a gastight seal. The effective area of oxygen permeation was 1.3 cm^2. COG (31.800% CH_4, 57.705% H_2, 7.366% CO, and 3.069% CO_2) and the air passed through the thin quartz tubes. These gases were placed at the location of 2 mm above or below the membrane in order to sweep the upper and lower surfaces of membrane, respectively. The gas flow rates were controlled by mass flow controllers.

Prior to the testing, gas tightness of membrane reactor was examined by detecting nitrogen in the outlet gas. A total of 1.0 g of 20–40 mesh $Mg_{0.7}Co_{0.3}O$ catalyst was directly placed on the upper surface. A K thermoelement measured the center temperature in the membrane reactor. On the permeation side of the membrane, the water was removed by $Mg(ClO_4)_2$, and H_2, CO, CO_2 and CH_4 in the outlet gas were analyzed by a Varian CP3800 gas chromatography (GC) with a thermal conductivity detector (TCD). According to the law of mass conservation, the oxygen permeation flux could be obtained as follows [15]:

$$F_{O_2,\text{inlet}} = \frac{1}{2}F_{CO,\text{outlet}} + F_{CO_2,\text{outlet}} + F_{CH_4,\text{inlet}} - F_{CH_4,\text{outlet}} - \frac{1}{2}\left(F_{H_2,\text{outlet}} - F_{H_2,\text{inlet}}\right) - \frac{1}{2}F_{CO,\text{inlet}} - F_{CO_2,\text{inlet}}, \quad (1)$$

where $F_{i,\text{inlet}}$ and $F_{i,\text{outlet}}$ are the flow rate (mL·min^{-1}) of the inlet and outlet gas I, respectively. $F_{O_2,\text{inlet}}$ is to be divided by the effective area of oxygen permeable membrane to obtain the actual oxygen permeation flux, J_{O_2}, mL·min^{-1}·cm^{-2}.

3. Results and Discussion

Figure 2 shows the XRD patterns of YDC nanopowders and BCFN powders. A single phase of cubic fluoride structure is obtained for YDC nanopowders in Figure 2(a). The pattern is indexed perfectly as $Ce_{0.8}Y_{0.2}O_{2-\delta}$ (JCPDS no. 75-0175). No other phase can be found which indicates that Y_2O_3 was homogeneously incorporated in the perovskite structure. Through the calculation of Scherrer's equation, the average crystallite size of YDC nanopowders is about 15 nm. In addition, a single perovskite structure of BCFN membrane can be also discovered according to the previous study [28] in Figure 2(b).

Since the oxygen membranes are used in high temperature environment, it is particularly important to study their high temperature stability. The BCFN ceramics modified by YDC layer showed the cubic fluoride structure and cubic perovskite structure (Figure 3(a)). However, the relative ceramics, which were prepared by simply mixing BCFN and YDC powders via ball-milling treatment and sintering at 1000°C for 5 h, displayed two obvious phases (Figure 3(b)). It means that the cubic fluoride structure and cubic perovskite structure are solely separated. The peaks of Figure 3(a) are lower than those of Figure 3(b) due to the YDC porous layer on the BCFN surface.

Obviously, the smaller nanoparticles can improve the oxygen permeability as they could enhance the effective specific surface area in YDC porous layer. Therefore, the microscopic structures of YDC nanopowders are characterized by TEM. Figure 4(a) illustrates that the YDC powders were well dispersed, and the particle size was around 10~25 nm. Additionally, it can be also found that the surfaces of BCFN ceramics are incredibly dense and composed of big particles with the crystal size of 5~20 μm (Figure 4(b)).

Regarding the coating materials, the adhesion between membrane and coated layers is very important for POM application. So the adhesion of BCFN membrane and YDC porous layer is studied by the ultrasonic vibration. Through analyzing the weight balance after calcination at different

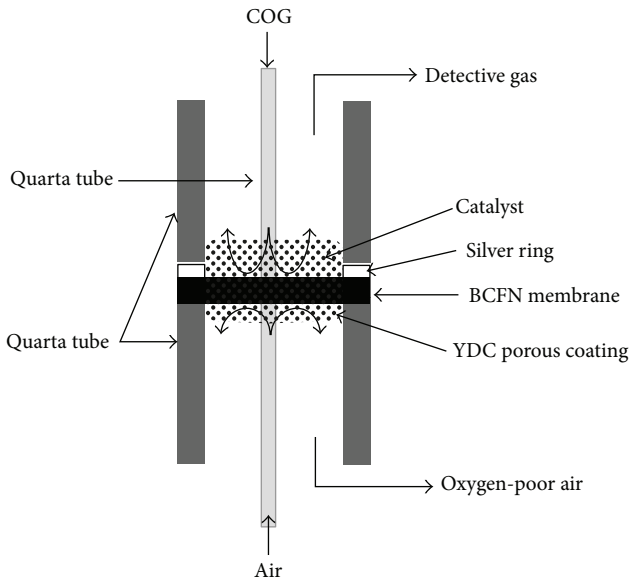

Figure 1: Schematic configuration of the membrane reactor at COG atmosphere.

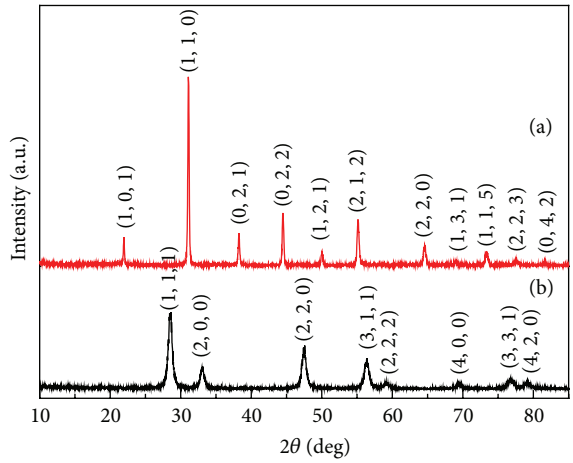

Figure 2: XRD patterns of (a) YDC nanopowders and (b) BCFN powders.

temperatures before and after ultrasonic treatments, the change trend of coating can be observed. It gradually reduced with the increment of calcination temperatures and altered smoothly above 950°C (Figure 5). The highest calcination temperature of BCFN-YDC is 1000°C in this paper.

The surface and cross section of BCFN-YDC samples are observed by SEM (Figure 6). The YDC layer exhibits a porous structure (Figures 6(a)–6(c)). These pores are accumulated by 100~200 nm YDC nanoparticle and should be caused by the volatilization of organic solution in the slurry. The boundary between BCFN dense membrane and YDC porous layer could be easily distinguished (Figure 6(d)). But the YDC porous layer was well adhered to the BCFN membrane and its thickness was around 5~6 μm.

Figure 7 showed the oxygen permeation flux of the BCFN membranes with and without YDC porous layer when COG flow rate changed at 875°C. It can be seen that the oxygen permeation flux increases with rising COG flow rate, which can be attributed to the decrease of oxygen partial pressure on the permeation side. Moreover, BCFN-YDC exhibited higher oxygen permeation flux than uncoated BCFN membrane. When the air flow and COG flow were 173 mL/min and 108 mL/min, respectively, the oxygen permeation flux of BCFN-YDC was achieved at 16.62 mL·min^{-1}·cm^{-2}, and it was about 23.5% higher than pure BFCN.

4. Conclusions

BCFN membrane modified by YDC porous on the air side formed a novel structure. A pure phase perovskite of BCFN membrane and a pure phase fluorite of YDC porous layer were obtained by dipping method. This novel structure exhibits higher stability and no chemical reaction at high temperature environment. In contrast to uncoated BCFN, it

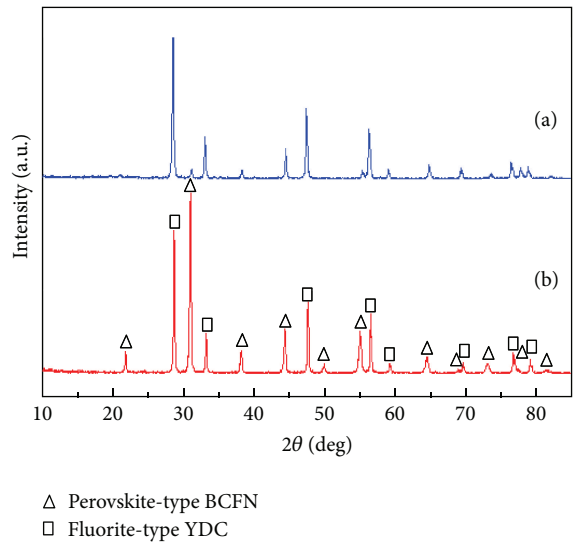

Figure 3: XRD patterns of (a) BCFN-YDC membrane and (b) the ceramics prepared by mixing BCFN and YDC powders.

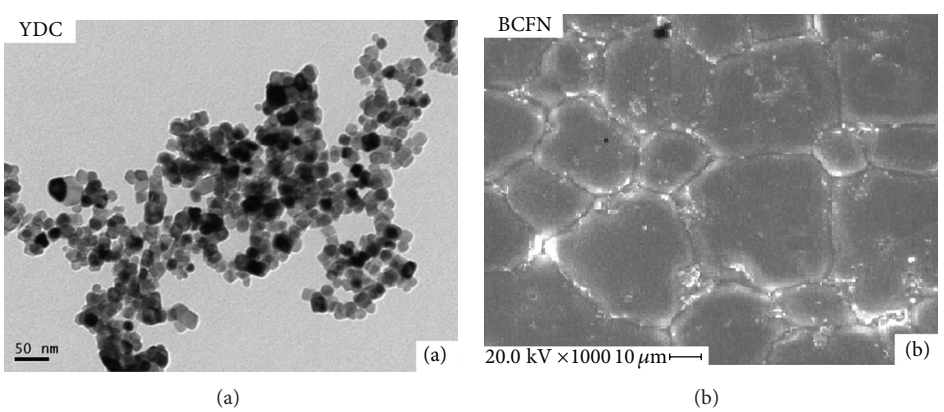

Figure 4: Images of (a) YDC nanopowders and (b) BCFN membrane.

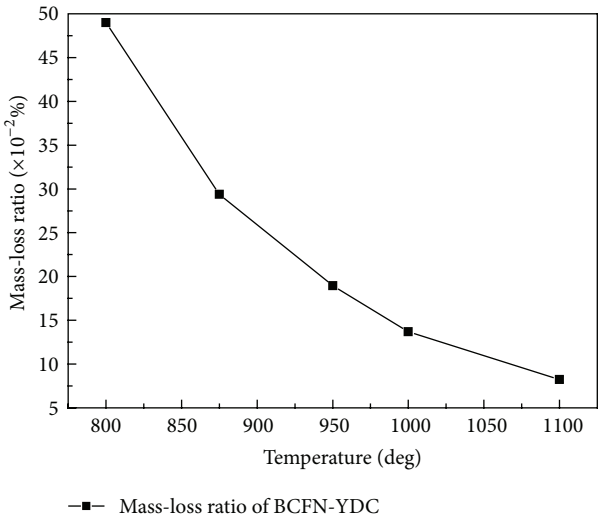

Figure 5: The change trend of YDC porous coating after calcination at different temperatures after ultrasonic treatments.

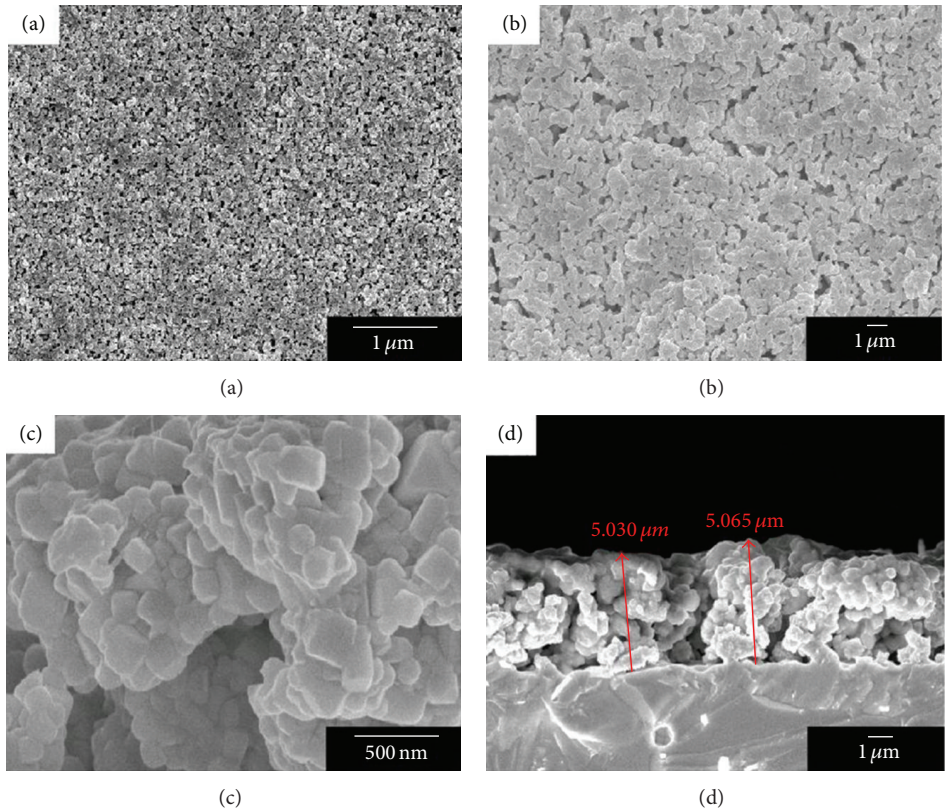

FIGURE 6: SEM images of ((a)–(c)) YDC porous layer at different magnification and (d) the cross-section of BCFN-YDC.

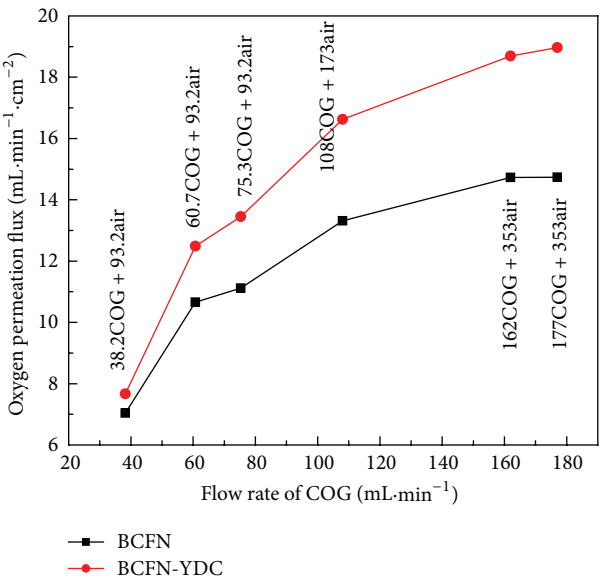

FIGURE 7: Oxygen permeation of BCFN and BCFN-YDC with COG changing at 875°C.

also obviously enhanced the oxygen permeation flux for COG application (23.5%). Our method may provide a new way for further improving oxygen permeation flux of COG.

Acknowledgment

The financial supports received from the National Natural Science Foundation of People's Republic of China (no. 51072112) are greatly appreciated.

References

[1] J. Shen, Z.-Z. Wang, H.-W. Yang, and R.-S. Yao, "A new technology for producing hydrogen and adjustable ratio syngas from coke ove gas," *Energy and Fuels*, vol. 21, no. 6, pp. 3588–3592, 2007.

[2] H. J. M. Bouwmeester, H. Kruidhof, and A. J. Burggraaf, "Importance of the surface exchange kinetics as rate limiting step in oxygen permeation through mixed-conducting oxides," *Solid State Ionics*, vol. 72, no. 2, pp. 185–194, 1994.

[3] M. Harada, K. Domen, M. Hara, and T. Tatsumi, "$Ba_{1.0}Co_{0.7}Fe_{0.2}Nb_{0.1}O_{3-\delta}$ dense ceramic as an oxygen permeable membrane for partial oxidation of methane to synthesis gas," *Chemistry Letters*, vol. 35, no. 12, pp. 1326–1327, 2006.

[4] Y. Cheng, H. Zhao, D. Teng, F. Li, X. Lu, and W. Ding, "Investigation of Ba fully occupied A-site $BaCo_{0.7}Fe_{0.3-x}Nb_xO_{3-\delta}$ perovskite stabilized by low concentration of Nb for oxygen permeation membrane," *Journal of Membrane Science*, vol. 322, no. 2, pp. 484–490, 2008.

[5] H. Cheng, X. Lu, Y. Zhang, and W. Ding, "Hydrogen production by reforming of simulated hot coke oven gas over nickel

catalysts promoted with lanthanum and cerium in a membrane reactor," *Energy and Fuels*, vol. 23, no. 6, pp. 3119–3125, 2009.

[6] Y. S. Lin, "Microporous and dense inorganic membranes: current status and prospective," *Separation and Purification Technology*, vol. 25, no. 1–3, pp. 39–55, 2001.

[7] R. W. Baker, "Future directions of membrane gas separation technology," *Industrial and Engineering Chemistry Research*, vol. 41, no. 6, pp. 1393–1411, 2002.

[8] J. Sunarso, S. Baumann, J. M. Serra et al., "Mixed ionic-electronic conducting (MIEC) ceramic-based membranes for oxygen separation," *Journal of Membrane Science*, vol. 320, no. 1-2, pp. 13–41, 2008.

[9] J. W. Stevenson, T. R. Armstrong, R. D. Carneim, L. R. Pederson, and W. J. Weber, "Electrochemical properties of mixed conducting perovskites $La_{1-x}M_xCo_{1-y}Fe_yO_{3-\delta}$ (M = Sr, Ba, Ca)," *Journal of the Electrochemical Society*, vol. 143, no. 9, pp. 2722–2729, 1996.

[10] T. Ishihara, T. Yamada, H. Arikawa, H. Nishiguchi, and Y. Takita, "Mixed electronic-oxide ionic conductivity and oxygen permeating property of Fe-, Co- or Ni-doped $LaGaO_3$ perovskite oxide," *Solid State Ionics*, vol. 135, no. 1–4, pp. 631–636, 2000.

[11] Z. P. Shao, G. X. Xiong, J. H. Tong et al., "Ba effect in doped $Sr(Co_{0.8}Fe_{0.2})O_{3-\delta}$ on the phase structure and oxygen permeation properties of the dense ceramic membranes," *Separation and Purification Technology*, vol. 25, no. 1–3, pp. 419–429, 2001.

[12] H. Wang, Y. Cong, and W. Yang, "Investigation on the partial oxidation of methane to syngas in a tubular $Ba_{0.5}Sr_{0.5}Co_{0.8}Fe_{0.2}O_{3-\delta}$ membrane reactor," *Catalysis Today*, vol. 82, no. 1–4, pp. 157–166, 2003.

[13] S. Liu and G. R. Gavalas, "Oxygen selective ceramic hollow fiber membranes," *Journal of Membrane Science*, vol. 246, no. 1, pp. 103–108, 2005.

[14] W. Jin, S. Li, P. Huang, N. Xu, and J. Shi, "Preparation of an asymmetric perovskite-type membrane and its oxygen permeability," *Journal of Membrane Science*, vol. 185, no. 2, pp. 237–243, 2001.

[15] S. M. Murphy, D. A. Slade, K. J. Nordheden, and S. M. Stagg-Williams, "Increasing oxygen flux through a dense oxygen permeable membrane by photolithographic patterning of platinum," *Journal of Membrane Science*, vol. 277, no. 1-2, pp. 94–98, 2006.

[16] A. Thursfield and I. S. Metcalfe, "Air separation using a catalytically modified mixed conducting ceramic hollow fibre membrane module," *Journal of Membrane Science*, vol. 288, no. 1-2, pp. 175–187, 2007.

[17] A. Leo, S. Liu, J. C. Diniz da Costa, and Z. Shao, "Oxygen permeation through perovskite membranes and the improvement of oxygen flux by surface modification," *Science and Technology of Advanced Materials*, vol. 7, no. 8, pp. 819–825, 2006.

[18] S. Li, L. Ge, H. Gu, Y. Zheng, H. Chen, and L. Guo, "Sinterability and electrical properties of ZnO-doped $Ce_{0.8}Y_{0.2}O_{1.9}$ electrolytes prepared by an EDTA-citrate complexing method," *Journal of Alloys and Compounds*, vol. 509, no. 1, pp. 94–98, 2011.

[19] Q. Zhen, Q. Yuan, H. Wang, C. Ding, W. Ding, and X. Lu, "Investigation of chemical stability and oxygen permeability of perovskite-type $Ba_{0.5}Sr_{0.5}Co_{0.8}Fe_{0.2}O_{3-\delta}$ and $BaCo_{0.7}Fe_{0.2}Nb_{0.1}O_{3-\delta}$ ceramic membranes," *Solid State Ionics*, vol. 198, no. 6, pp. 50–55, 2011.

[20] B. C. H. Steele, "Appraisal of $Ce_{1-y}GdyO_{2-y/2}$ electrolytes for IT-SOFC operation at 500°C," *Solid State Ionics*, vol. 129, no. 1, pp. 95–110, 2000.

[21] M. Mogensen, N. M. Sammes, and G. A. Tompsett, "Physical, chemical and electrochemical properties of pure and doped ceria," *Solid State Ionics*, vol. 129, no. 1, pp. 63–94, 2000.

[22] Q. Yuan, Q. Zhen, R. Li, L. Gao, and L. Ni, "Reaction mechanism of preparing $Bi_{0.75}Dy_{0.25}O_{1.5}$ nanopowder by the reverse titration chemical coprecipitation method," *Journal of University of Science and Technology Beijing*, vol. 32, no. 2, pp. 245–249, 2010.

[23] Q. Zhen, G. M. Kale, G. Shi et al., "Processing of dense nanocrystalline Bi_2O_3-Y_2O_3 solid electrolyte," *Solid State Ionics*, vol. 176, no. 30, pp. 2727–2733, 2005.

[24] Q. Zhen, R. N. Vannier, and G. M. Kale, "Preparation of dense nanocrystalline Bi_2O_3-HfO_2-Y_2O_3 ceramic by microwave plasma sintering," *Materials Science and Engineering A*, vol. 444, no. 1-2, pp. 130–137, 2007.

[25] N. N. Dinh, N. T. T. Oanh, P. D. Long et al., "Electrochromic properties of TiO_2 anatase thin films prepared by a dipping sol-gel method," *Thin Solid Films*, vol. 423, no. 1, pp. 70–76, 2003.

[26] E. Barrera, T. Viveros, A. Avila et al., "Cobalt oxide films grown by a dipping sol-gel process," *Thin Solid Films*, vol. 346, no. 1-2, pp. 138–144, 1999.

[27] H. Hayashi, H. Inaba, M. Matsuyama, N. G. Lan, M. Dokiya, and H. Tagawa, "Structural consideration on the ionic conductivity of perovskite-type oxides," *Solid State Ionics*, vol. 122, no. 1–4, pp. 1–15, 1999.

[28] Y. Eraoka, M. Yoshimatsu, N. Yamazoe, and T. Seiyama, "Oxygen-sorptive properties and defect structure of perovskite-type oxides," *Chemistry Letters*, vol. 6, pp. 893–896, 1984.